

Nodal superconductivity and superconducting domes in the topological Kagome metal CsV₃Sb₅

C. C. Zhao^{1,6}, L. S. Wang^{1,6}, W. Xia^{2,3,6}, Q. W. Yin^{4,6}, J. M. Ni¹, Y. Y. Huang¹, C. P. Tu¹,
Z. C. Tao², Z. J. Tu⁴, C. S. Gong⁴, H. C. Lei^{4,+}, Y. F. Guo^{2,‡}, X. F. Yang^{1,#}, and S. Y. Li^{1,5*}

¹ State Key Laboratory of Surface Physics, Department of Physics, Fudan University, Shanghai 200438, China.

² School of Physical Science and Technology, ShanghaiTech University, Shanghai 201210, China.

³ ShanghaiTech Laboratory for Topological Physics, Shanghai 201210, China.

⁴ Department of Physics and Beijing Key Laboratory of Opto-electronic Functional Materials and Micro-nano Devices, Renmin University of China, Beijing 100872, China.

⁵ Shanghai Research Center for Quantum Sciences, Shanghai 201315, China.

⁶ These authors contributed equally.

Corresponding author. Email: hlei@ruc.edu.cn (H.C.L); guoyf@shanghaitech.edu.cn (Y.F.G);
yangxiaofan@fudan.edu.cn (X.F.Y.); shiyan_li@fudan.edu.cn (S.Y.L.)

Abstract

Recently superconductivity was discovered in the Kagome metal AV_3Sb_5 ($A = K, Rb,$ and Cs), which has an ideal Kagome lattice of vanadium. These V-based superconductors also host charge density wave (CDW) and topological nontrivial band structure. Here we report the ultralow-temperature thermal conductivity and high pressure resistance measurements on CsV_3Sb_5 with $T_c \approx 2.5$ K, the highest among AV_3Sb_5 . A finite residual linear term of thermal conductivity at zero magnetic field and its rapid increase in fields suggest nodal superconductivity. By applying pressure, the T_c of CsV_3Sb_5 increases first, then decreases to lower than 0.3 K at 11.4 GPa, showing a clear first superconducting dome peaked around 0.8 GPa. Above 11.4 GPa, superconductivity re-emerges, suggesting a second superconducting dome. Both nodal superconductivity and superconducting domes point to unconventional superconductivity in this

V-based superconductor. While our finding of nodal superconductivity puts a strong constrain on the pairing state of the first dome, which should be related to the CDW instability, the superconductivity of the second dome may present another exotic pairing state in this ideal Kagome lattice of vanadium.

Introduction

Finding unconventional superconductors and understanding their superconducting mechanism is the frontier of condensed matter physics, e.g., the heavy-fermion superconductors, Cu-based and Fe-based high-temperature superconductors¹, and recent Ni-based superconductors². Unlike the conventional *s*-wave superconductors, the wave function of Cooper pairs for unconventional superconductors is usually not *s*-wave. Symmetry imposed nodes (gap zeros) are often observed, such as in *d*-wave cuprate superconductors and heavy-fermion superconductor CeCoIn₅ (ref. ^{3,4}). Note that the Fe-based superconductors are exceptions, in which both multiple *s*-wave gaps and nodal gaps are found⁵. Furthermore, the superconducting pairing mechanism of unconventional superconductors is not phonon-mediated. This usually manifests as a superconducting dome neighbouring a magnetic order or density-wave order in the phase diagram, and spin or density-wave fluctuations are considered as the major pairing glue¹. The superconducting gap structure and superconducting dome nearby an ordered state provide important clues to the underlying pairing mechanism.

Recently, superconductivity was discovered in a new family of V-based compounds AV_3Sb_5 ($A = K, Rb, \text{ and } Cs$)⁶⁻⁹. These compounds have the ideal Kagome lattice of vanadium coordinated by antimony, with the A atoms intercalated between the layers, as seen in Fig. 1a and 1b. The superconducting transition temperature T_c is 0.93, 0.92, and 2.5 K for $A = K, Rb, \text{ and } Cs$, respectively⁷⁻⁹. While there are no local magnetic moments¹⁰, these V-based superconductors manifest a charge density wave (CDW) order at 78, 103, and 94 K, respectively⁶⁻⁹. Interestingly, for KV₃Sb₅, high-resolution scanning tunneling microscopy (STM) study demonstrated that such charge order in the frustrated Kagome lattice is topological¹¹, which leads to a giant anomalous Hall effect¹², and can also be a strong precursor of unconventional superconductivity¹¹. Moreover, topological nontrivial band structures, including multiple Dirac points and possible surface state, were revealed by angle-resolved photoemission spectroscopy (ARPES) measurements combined with density-functional theory (DFT)

calculations^{7,12}. In this context, the Kagome metal AV_3Sb_5 provides a great platform to study the interplay of superconductivity, CDW, frustration, and topology. It will be very important to understand the superconducting state first.

In this paper, we present ultralow-temperature thermal conductivity measurements of CsV_3Sb_5 single crystal to investigate its superconducting gap structure. The data in zero and magnetic fields clearly demonstrate that there are nodes in the superconducting gap. Furthermore, two superconducting domes in the temperature-pressure phase diagram are revealed by resistance measurement under pressures up to 47.0 GPa. These results suggest unconventional superconductivity in CsV_3Sb_5 . We discuss the possible novel superconducting states in these V-based superconductors.

Results and discussion

Figure 1c plots the XRD pattern of CsV_3Sb_5 single crystal, showing that the largest natural face is (00l) plane. In Fig. 1d, the magnetization measured in 1 T with zero-field and field cooling modes displays a sharp drop at 94 K, which is the CDW transition reported previously⁷. The low-temperature magnetic susceptibility measured at 10 Oe with zero-field and field cooling modes is plotted in Fig. 2a. The onset of the superconductivity is at 2.5 K, which is also consistent with previous report⁷.

In Fig. 2b, we present the temperature dependence of in-plane resistivity for CsV_3Sb_5 single crystal in magnetic fields up to 2 T. In zero field, the T_c defined at 10% drop of normal-state resistivity ($T_c^{10\%}$) and zero resistivity (T_c^{zero}) are 3.6 K and 2.7 K, respectively. The T_c^{zero} is slightly higher than the onset T_c from magnetic susceptibility measurement. The normal-state resistivity shows a very weak temperature dependence below 6 K. A simple extrapolation gives residual resistivity $\rho_0(0T) = 4.75 \mu\Omega$ cm and $\rho_0(0.2T) = 4.82 \mu\Omega$ cm, respectively. The temperature dependence of H_{c2} , determined by the T_c^{zero} values in Fig. 2b, is plotted in Fig. 2c. The red line is a linear fit to $\mu_0 H_{c2}(T)$, and $\mu_0 H_{c2}(0) \approx 0.47$ T is roughly estimated.

The ultralow-temperature heat transport measurement is an established bulk technique to probe the superconducting gap structure¹³. Figure 3 presents the in-plane thermal conductivity results of CsV_3Sb_5 single crystal. At very low temperatures, the thermal conductivity can usually be fitted to $\kappa/T = a + bT^{\alpha-1}$ (ref. ^{14,15}), in which the two terms aT and bT^α represent contributions from electrons and phonons, respectively. The power a is typically between 2 and 3, due to specular reflections of phonons at the

boundary^{14,15}. In zero field, the fitting of the data below 0.5 K gives a finite residual linear term $\kappa_0/T \equiv a = 0.22 \pm 0.04 \text{ mW K}^{-2} \text{ cm}^{-1}$ and $\alpha = 2.70 \pm 0.12$. Figure 3a is plotted as κ/T vs $T^{1.70}$ to show the data more clearly.

For *s*-wave nodeless superconductors, there are no fermionic quasiparticles to conduct heat as $T \rightarrow 0$, since the Fermi surface is entirely gapped. Therefore, there is no residual linear term κ_0/T , as seen in InBi and NbSe₂ (ref. ^{16,17}). However, for nodal superconductors, a substantial κ_0/T in zero field contributed by the nodal quasiparticles can be found¹³. For example, κ_0/T of the overdoped ($T_c = 15 \text{ K}$) *d*-wave cuprate superconductor Tl₂Ba₂CuO_{6+ δ} (Tl-2201) is $1.41 \text{ mW K}^{-2} \text{ cm}^{-1}$, which is about 36% of the normal-state value κ_{N0}/T (ref. ¹⁸), and $\kappa_0/T = 17 \text{ mW K}^{-2} \text{ cm}^{-1}$ for Sr₂RuO₄, which is about 9% of its κ_{N0}/T (ref. ¹⁹). For clean Fe-based superconductor KFe₂As₂, $\kappa_0/T = 3.8 \text{ mW K}^{-2} \text{ cm}^{-1}$ is about 3.2% of the normal-state value κ_{N0}/T (ref. ²⁰). For ultraclean YBa₂Cu₃O₇ (i.e., very low ρ_0 and very high κ_{N0}/T in the normal state), $\kappa_0/T = 0.16 \text{ mW K}^{-2} \text{ cm}^{-1}$ is a universal value for *d*-wave superconducting gap²¹. Therefore, the finite $\kappa_0/T = 0.22 \text{ mW K}^{-2} \text{ cm}^{-1}$ of CsV₃Sb₅ in zero field is a strong evidence for the presence of nodes in the superconducting gap¹³.

Further information on the superconducting gap structure can be obtained by examining the behavior of field-dependent κ_0/T (ref. ¹³). In Fig. 3b, the thermal conductivity of CsV₃Sb₅ in magnetic fields up to 0.25 T are plotted. By applying a very small field 0.01 T, one can see a large enhancement of thermal conductivity. Since all the curves in magnetic fields are roughly linear, we fix α to 2, thus fit the data to $\kappa/T = a + bT$ and obtain the κ_0/T for each magnetic field. For $\mu_0 H = 0.16 \text{ T}$, the fitting gives $\kappa_0/T = 4.15 \pm 0.13 \text{ mW K}^{-2} \text{ cm}^{-1}$. Further increasing field to 0.25 T does not increase the thermal conductivity, therefore we take 0.16 T as the bulk $H_{c2}(0)$. Note that this value is lower than that obtained from resistivity measurements. Interestingly, there is about 20% violation of Wiedemann-Franz law in the normal state, when we compare the κ_0/T at 0.16 T to its Wiedemann-Franz law expectation L_0/ρ_0 (0.16T) $\approx 5.08 \text{ mW K}^{-2} \text{ cm}^{-1}$, with the Lorenz number $L_0 = 2.45 \times 10^{-8} \text{ W } \Omega \text{ K}^{-2}$ and $\rho_0(0.16\text{T}) \approx \rho_0(0.20\text{T}) = 4.82 \mu\Omega \text{ cm}$. The origin of this violation is not clear to us at this stage. It may come from the topological nontrivial band structure, i.e., either the Dirac quasiparticles violate the Wiedemann-Franz law, or the surface state conducts electrical current much better than the heat current. We leave this issue for future investigation.

The normalized values of $[\kappa_0/T]/[\kappa_{N0}/T]$ as a function of H/H_{c2} for CsV₃Sb₅ is plotted in Fig. 3c, with $\kappa_{N0}/T = 4.15 \text{ mW K}^{-2} \text{ cm}^{-1}$ and $H_{c2} = 0.16 \text{ T}$. For comparison, similar data of the clean *s*-wave

superconductor Nb (ref. ²²), the dirty *s*-wave superconducting alloy InBi (ref. ¹⁶), the multiband *s*-wave superconductor NbSe₂ (ref. ¹⁷), and an overdoped *d*-wave cuprate superconductor Tl-2201 (ref. ¹⁸), are also plotted. For CsV₃Sb₅, the field dependence of κ_0/T clearly mimics the behaviour of Tl-2201. The rapid increase of κ_0/T in magnetic field should come from the Volovik effect of nodal quasiparticles, thus provides further evidence for nodes in the superconducting gap¹³. To our knowledge, so far all nodal superconductors have unconventional pairing mechanism¹. In this regard, the nodal gap we demonstrate from thermal conductivity results suggests unconventional superconductivity in CsV₃Sb₅.

To get further clue to the pairing mechanism in CsV₃Sb₅, we map out its temperature-pressure phase diagram by resistance measurement under pressures. Figure 4a presents the low-temperature resistance of CsV₃Sb₅ single crystal under various pressures up to 11.4 GPa. At ambient pressure, the $T_c^{10\%}$ is 3.6 K. With increasing pressure, the $T_c^{10\%}$ first increases sharply to 5.6 K at 0.8 GPa, enhanced by 56%. Under this pressure, applying magnetic field gradually suppresses the superconducting transition, as shown in Fig. 4b. With further increasing pressure, $T_c^{10\%}$ decreases slowly to below 0.3 K at 11.4 GPa. The non-monotonic pressure dependence of $T_c^{10\%}$ is plotted in Fig. 4c, which shows a clear superconducting dome. Since the CDW usually competes with superconductivity, it is expected that the CDW order may be suppressed near the optimal pressure $p_c \sim 0.8$ GPa of the superconducting dome. This needs to be examined by high pressure magnetization measurements. More interestingly, as the pressure further increases, superconductivity re-emerges, and the T_c keeps increasing up to 47.0 GPa, as shown in Fig. 4d. The effect of field on the resistance transition under 29.3 GPa in Fig. 4e demonstrates it is a superconducting transition. In Fig. 4f, we plot the full temperature – pressure phase diagram, which includes two superconducting domes.

A temperature - pressure (T_c vs p) or temperature - doping (T_c vs x) superconducting dome has been commonly observed in many unconventional superconductors, including heavy-fermion superconductors, cuprate superconductors, iron-based superconductors, and quasi-two-dimensional organic superconductors¹. For example, the heavy-fermion superconductor CeCoIn₅ manifests a T_c vs p superconducting dome, and the unconventional superconductivity with $d_{x^2-y^2}$ symmetry may result from the antiferromagnetic spin fluctuations²³. Theoretically, it has been shown that unconventional superconductivity with d_{xy} symmetry can also appear in close proximity to a charge-ordered phase, and the superconductivity is mediated by charge fluctuations^{24,25}. This may be the case

of the pressure-induced superconductivity in $1T$ -TiSe₂, with the superconducting dome appearing around the critical pressure related to the charge-density wave (CDW) meltdown²⁶. For Kagome lattice at van Hove filling, previous theoretical calculations found competing electronic orders, including CDW and chiral $d_{x^2-y^2} + id_{xy}$ superconductivity^{27,28}. However, proximity-induced spin-triplet superconductivity was claimed in Nb-K_{1-x}V₃Sb₅ devices²⁹. Nevertheless, our finding of nodal superconductivity put a strong constrain on the pairing state of the first dome of CsV₃Sb₅, which should be related to the CDW instability. A second superconducting dome is rare, including the heavy-fermion CeCu₂(Si_{1-x}Ge_x)₂ (ref. ³⁰) and the iron chalcogenides³¹. Since the second dome is away from the CDW order, more experimental and theoretical works are needed to understand the superconductivity of the second dome in CsV₃Sb₅.

In summary, we investigate the superconducting gap structure of the new V-based superconductor CsV₃Sb₅ by ultralow-temperature thermal conductivity measurements. The finite κ_0/T in zero magnetic field and its rapid field dependence give strong evidences for nodes in the superconducting gap. Further measurements of resistance under pressure reveal two superconducting domes in the temperature - pressure phase diagram. These results suggest unconventional superconductivity in CsV₃Sb₅. While our finding of nodal superconductivity puts a strong constrain on the pairing state of the first dome, which should be related to the CDW instability, the superconductivity of the second dome may present another exotic pairing state in this ideal Kagome lattice of vanadium.

Methods

Sample preparation. Single crystals of CsV₃Sb₅ were grown from Cs ingot (purity 99.9%), V powder (purity 99.9%) and Sb grains (purity 99.999%) using the self-flux method⁷. The eutectic mixture of CsSb and CsSb₂ is mixed with VSb₂ to form a composition with 50 at.% Cs_xSb_y and 50 at.% VSb₂ approximately. The mixture was put into an alumina crucible and sealed in a quartz ampoule under partial argon atmosphere. The sealed quartz ampoule was heated to 1273 K for 12 h and soaked there for 24 h. Then it was cooled down to 1173 K at 50 K/h and further to 923 K at a slowly rate. Finally, the ampoule was taken out from the furnace and decanted with a centrifuge to separate CsV₃Sb₅ single crystals from the flux. CsV₃Sb₅ single crystals are stable in the air. The X-ray diffraction (XRD) measurement was performed on a typical CsV₃Sb₅ sample by using an X-ray diffractometer (D8 Advance, Bruker), and determined the largest surface to be the (00 l) plane.

DC magnetization measurement. The DC magnetization measurement was performed down to 1.8 K using a magnetic property measurement system (MPMS, Quantum Design).

Resistivity and thermal transport measurements. The sample with dimensions of $1.96 \times 0.27 \text{ mm}^2$ in the ab plane and a thickness of $57 \text{ }\mu\text{m}$ along the c axis was used for both resistivity and thermal transport measurements at ambient pressure. Four silver wires were attached to the sample with silver paint, which were used for both resistivity and thermal conductivity measurements under ambient pressure, with electrical and heat currents in the ab plane. The in-plane resistivity was measured in a ^3He cryostat. The in-plane thermal conductivity was measured in a dilution refrigerator by using a standard four-wire steady-state method with two RuO_2 chip thermometers, calibrated *in situ* against a reference RuO_2 thermometer. Magnetic fields were applied perpendicular to the ab plane in all measurements. To ensure a homogeneous field distribution in the sample, all fields for resistivity and thermal conductivity measurements were applied at a temperature above T_c .

High pressure measurements. High pressure resistance of CsV_3Sb_5 powder sample (ground from single crystals) was measured in a physical property measurement system (PPMS, Quantum Design) and a ^3He cryostat by using a diamond anvil cell (DAC). The pressures inside of the DAC were scaled by ruby fluorescence method at room temperature each time before and after the measurement.

Data availability

The data that support the findings of this study are available from the corresponding author upon reasonable request.

References

1. Norman, M. R. The Challenge of Unconventional Superconductivity. *Science* **332**, 196-200 (2011).
2. Li, D. et al. Superconductivity in an infinite-layer nickelate. *Nature* **572**, 624-627 (2019).
3. Tsuei, C. C. & Kirtley, J. R. Pairing symmetry in cuprate superconductors. *Rev. Mod. Phys.* **72**, 969 (2000).
4. An, K. et al. Sign Reversal of Field-Angle Resolved Heat Capacity Oscillations in a Heavy Fermion Superconductor CeCoIn_5 and $d_x^2-y^2$ Pairing Symmetry. *Phys. Rev. Lett.* **104**, 037002 (2010).
5. Chen, X. H., Dai, P. C., Feng, D. L., Xiang, T. & Zhang, F. C. Iron-based high transition temperature superconductors. *Natl. Sci. Rev.* **1**, 371-395 (2014).
6. Ortiz, B. R. et al. New kagome prototype materials: discovery of KV_3Sb_5 , RbV_3Sb_5 , and CsV_3Sb_5 . *Phys. Rev. Mater.* **3**, 094407 (2019).

7. Ortiz, B. R. et al. CsV₃Sb₅: A Z₂ Topological Kagome Metal with a Superconducting Ground State. *Phys. Rev. Lett.* **125**, 247002 (2020).
8. Ortiz, B. R. & Sarte, P. M. Superconductivity in the Z₂ kagome metal KV₃Sb₅. arXiv: 2012.09097.
9. Yin, Q., Tu, Z., Gong, C., Fu, Y., Yan, S. & Lei, H. Superconductivity and normal-state properties of kagome metal RbV₃Sb₅ single crystals. arXiv: 2101.10193.
10. Kenney, E. M., Ortiz, B. R., Wang, C., Wilson, S. D. & Graf, M. J. Absence of local moments in the kagome metal KV₃Sb₅ as determined by muon spin spectroscopy. arXiv: 2012.04737.
11. Jiang, Y.-X. et al. Discovery of topological charge order in kagome superconductor KV₃Sb₅. arXiv: 2012.15709.
12. Yang, S.-Y. et al. Giant, unconventional anomalous Hall effect in the metallic frustrated magnet candidate, KV₃Sb₅. *Sci. Adv.* **6**, 6003 (2020).
13. Shakeripour, H., Petrovic, C. & Taillefer, L. Heat transport as a probe of superconducting gap structure. *New J. Phys.* **11**, 055065 (2009).
14. Sutherland, M. et al. Thermal conductivity across the phase diagram of cuprates: Low-energy quasiparticles and doping dependence of the superconducting gap. *Phys. Rev. B* **67**, 174520 (2003).
15. Li, S. Y. et al. Low-temperature phonon thermal conductivity of single-crystalline Nd₂CuO₄: Effects of sample size and surface roughness. *Phys. Rev. B* **77**, 134501 (2008).
16. Willis, J. O. & Ginsberg, D. M. Thermal conductivity of superconducting alloy films in a perpendicular magnetic field. *Phys. Rev. B* **14**, 1916 (1976).
17. Boaknin, E. et al. Heat Conduction in the Vortex State of NbSe₂: Evidence for Multiband Superconductivity. *Phys. Rev. Lett.* **90**, 117003 (2003).
18. Proust, C., Boaknin, E., Hill, R. W., Taillefer, L. & Mackenzie, A. P. Heat Transport in a Strongly Overdoped Cuprate: Fermi Liquid and a Pure d-Wave BCS Superconductor. *Phys. Rev. Lett.* **89**, 147003 (2002).
19. Suzuki, M. et al. Universal Heat Transport in Sr₂RuO₄. *Phys. Rev. Lett.* **88**, 227004 (2002).
20. Reid, J.-Ph. et al. Universal Heat Conduction in the Iron Arsenide Superconductor KFe₂As₂: Evidence of a d-Wave State. *Phys. Rev. Lett.* **109**, 087001 (2012).
21. Hill, R. W. et al. Transport in Ultraclean YBa₂Cu₃O₇: Neither Unitary nor Born Impurity Scattering, *Phys. Rev. Lett.* **92**, 027001 (2004).
22. Lowell, J. & Sousa, J. B. Mixed-state thermal conductivity of type II superconductors. *J. Low Temp. Phys.* **3**, 65-87 (1970).
23. Sidorov, V. A. et al. Superconductivity and Quantum Criticality in CeCoIn₅. *Phys. Rev. Lett.* **89**, 157004 (2002).

24. Scalapino, D. J., Loh, E. & Hirsch, J. E. Fermi-surface instabilities and superconducting d-wave pairing. *Phys. Rev. B* **35**, 6694-6698 (1987).
25. Merino, J. & McKenzie, R. H. Superconductivity Mediated by Charge Fluctuations in Layered Molecular Crystals. *Phys. Rev. Lett.* **87**, 237002 (2001).
26. Kusmartseva, A. F., Sipos, B., Berger, H., Forró, L. & Tutiš, E. Pressure Induced Superconductivity in Pristine 1T-TiSe₂. *Phys. Rev. Lett.* **103**, 236401 (2009).
27. Wang, W.-S., Li, Z.-Z., Xiang, Y.-Y. & Wang, Q.-H. Competing electronic orders on kagome lattices at van Hove filling. *Phys. Rev. B* **87**, 115135 (2013).
28. Yu, Shun-Li and Li Jian-Xin, Chiral superconducting phase and chiral spin-density-wave phase in a Hubbard model on the kagome lattice. *Phys. Rev. B* **85**, 144402 (2012).
29. Wang, Y. et al. Proximity-induced spin-triplet superconductivity and edge supercurrent in the topological Kagome metal, K_{1-x}V₃Sb₅. arXiv: 2012.05898.
30. Yuan, H. Q., Grosche, F. M., Deppe, M., Geibel, C., Sparn, G., Steglich, F. Observation of Two Distinct Superconducting Phases in CeCu₂Si₂. *Science* **302**, 2104 (2003).
31. Sun, L. L., Chen, X. J., Guo, J., Gao, P. W., Huang, Q. Z., Wang, H. D., Fang, M. H., Chen, X. L., Chen, G. F., Wu, Q., Zhang, C., Gu, D. C., Dong, X. L., Wang, L., Yang, K., Li, A. G., Dai, X., Mao, H. K., Zhao, Z. X. Re-emerging superconductivity at 48 kelvin in iron chalcogenides. *Nature* **483**, 67 (2012).

Acknowledgements

This work was supported by the Natural Science Foundation of China (Grant No. 12034004), the Ministry of Science and Technology of China (Grant No.: 2016YFA0300503), and the Shanghai Municipal Science and Technology Major Project (Grant No. 2019SHZDZX01). Y. F. Guo was supported by the Major Research Plan of the National Natural Science Foundation of China (No. 92065201) and the Program for Professor of Special Appointment (Shanghai Eastern Scholar). H. C. Lei was supported by National Natural Science Foundation of China (Grant No. 11822412 and 11774423), the Ministry of Science and Technology of China (Grant No. 2018YFE0202600 and 2016YFA0300504), and Beijing Natural Science Foundation (Grant No. Z200005).

Author Contributions

S.Y.L. conceived the idea and designed the experiments. C.C.Z and L.S.W. performed the DC magnetization and bulk transport measurements with help from J.M.N., Y.Y.H., C.P.T., X.F.Y. was responsible for high-pressure transport experiments. W.X., Z.C.T., Y.F.G., Q.W.Y., Z.J.T., C.S.G., and H.C.L. synthesized the single crystal samples. S.Y.L. wrote the manuscript with comments from all authors. C.C.Z., L.S.W., W.X., and Q.W.Y. contributed equally to this work.

Competing interests

The authors declare no competing interests.

Additional information

Supplementary information is available for this paper at URL inserted when published

Correspondence and requests for materials should be addressed to H.C.L (hlei@ruc.edu.cn); Y.F.G

(guoyf@shanghaitech.edu.cn); X.F.Y. (yangxiaofan@fudan.edu.cn) or S.Y. L. (shiyang_li@fudan.edu.cn)

Figure 1

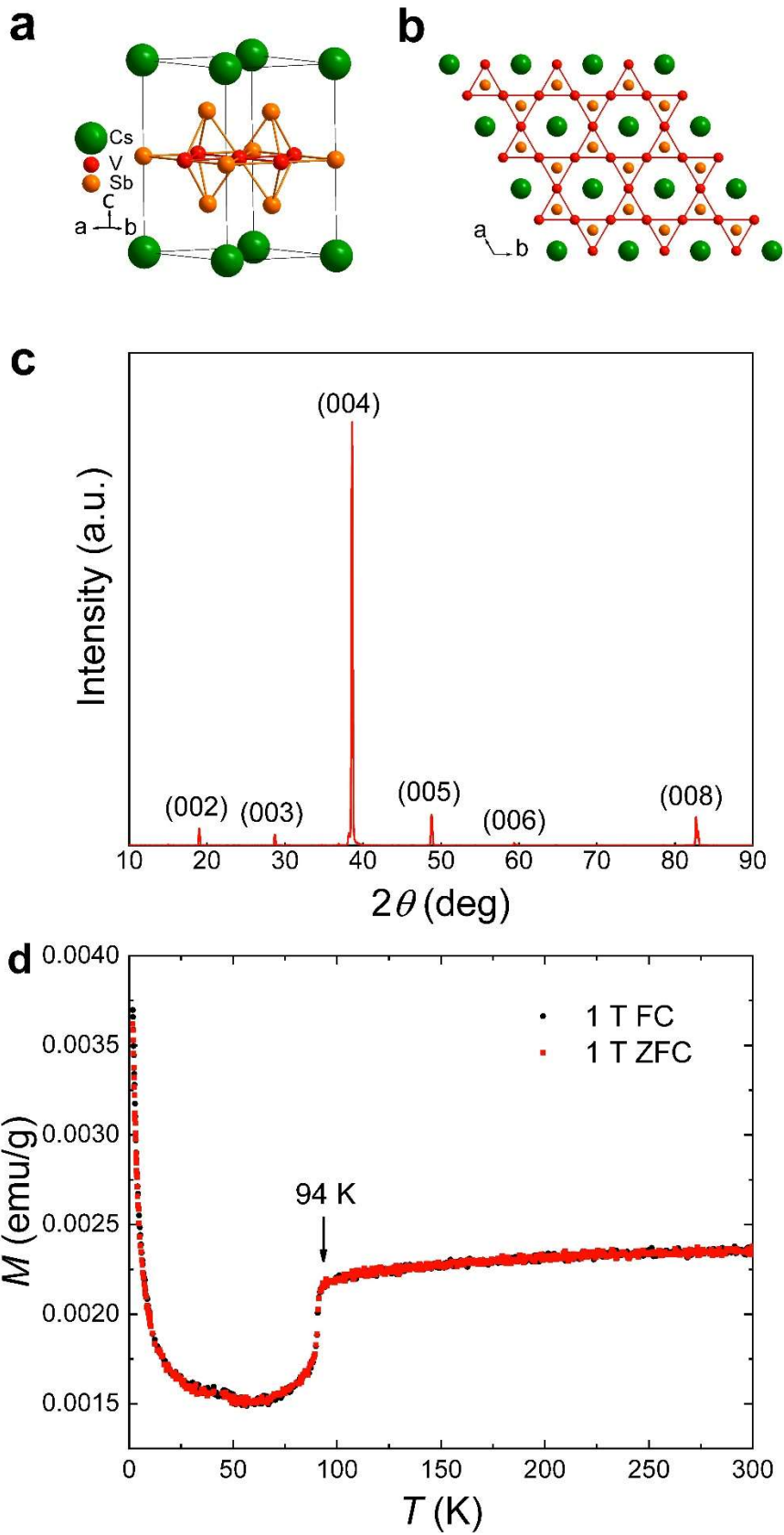


Figure 2

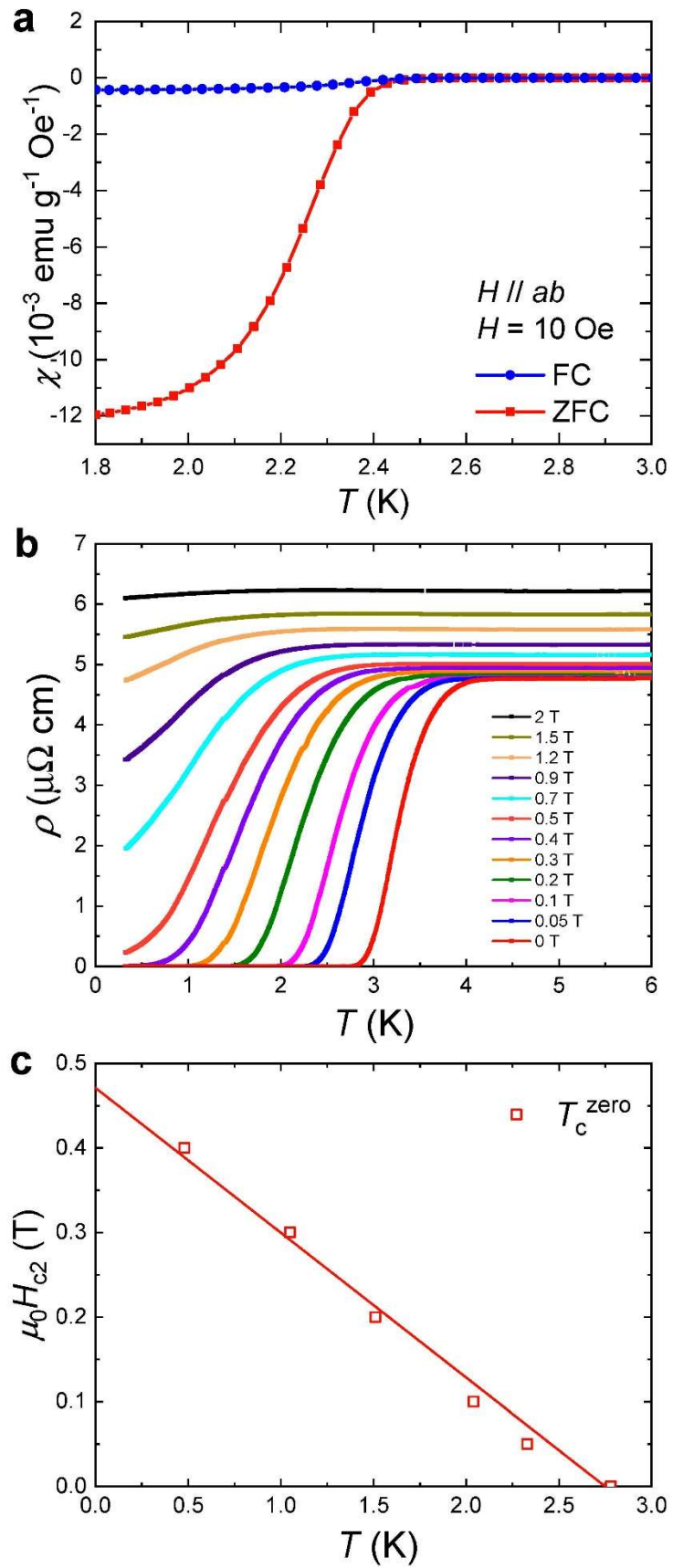


Figure 3

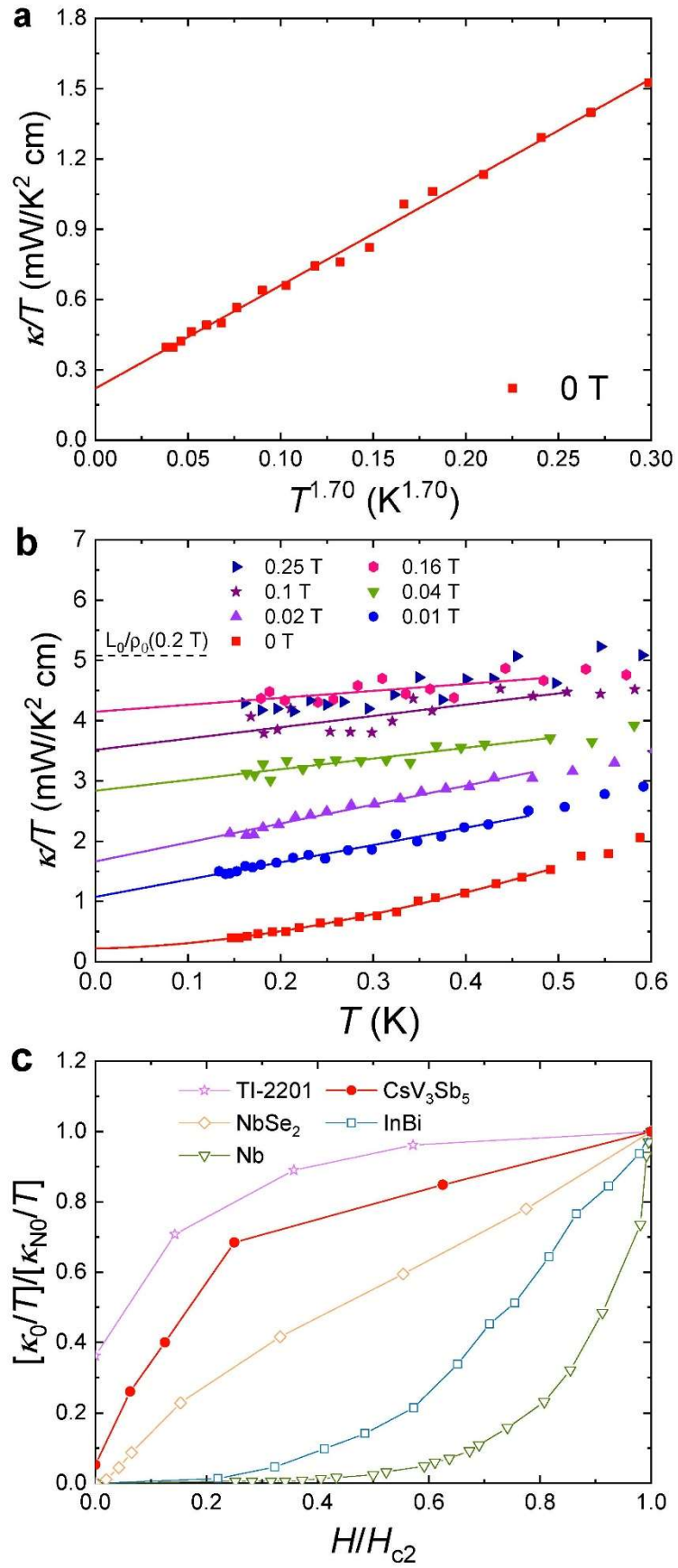


Figure 4

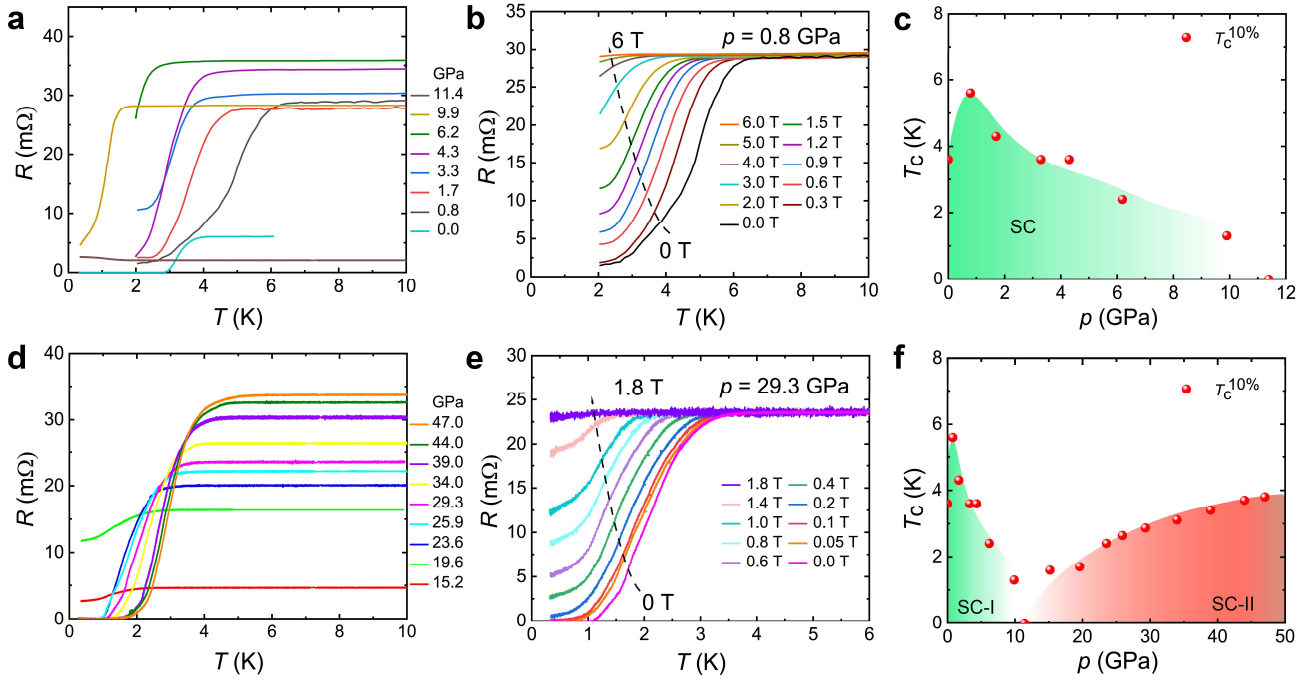


Figure captions

Fig. 1 | Characterization of CsV₃Sb₅. **a** Crystal structure of CsV₃Sb₅. The Cs, V, Sb atoms are presented as green, red and orange balls, respectively. **b** Top-down view of the crystal structure. The two-dimensional Kagome lattice of vanadium can be clearly seen. **c** Room-temperature X-ray diffraction pattern of the CsV₃Sb₅ single crystal, showing that the largest natural face is (00 l) plane. **d** Temperature dependence of the magnetization for CsV₃Sb₅ single crystal. The arrow denotes a charge density wave order at 94 K.

Fig. 2 | Superconductivity of CsV₃Sb₅. **a** Low-temperature magnetization of CsV₃Sb₅ single crystal at $H = 10$ Oe, with zero-field and field cooling modes, respectively. **b** Low-temperature in-plane resistivity of CsV₃Sb₅ single crystal in magnetic fields up to 2 T. **c** Temperature dependence of the upper critical field $\mu_0 H_{c2}$, extracted from the T_c^{zero} values in panel **b**. The red line is a linear fit to $\mu_0 H_{c2}(T)$, and $\mu_0 H_{c2}(0) \approx 0.47$ T is roughly estimated.

Fig. 3 | Thermal conductivity of CsV₃Sb₅. **a** Temperature dependence of the in-plane thermal conductivity for CsV₃Sb₅ single crystal in zero field. The solid line represents a fit to $\kappa/T = a + bT^{\alpha-1}$ below 0.5 K, which gives the residual linear term $\kappa_0/T \equiv a = 0.22 \pm 0.04$ mW K⁻² cm⁻¹ and $\alpha = 2.70 \pm 0.12$. **b** The thermal conductivity of CsV₃Sb₅ in magnetic fields up to 0.25 T. The dashed line is the normal-state Wiedemann-Franz law expectation L_0/ρ_0 (0.2T), with the Lorenz number 2.45×10^{-8} W Ω K⁻² and $\rho_0(0.2\text{T}) = 4.82$ $\mu\Omega$ cm. **c** Normalized residual linear term κ_0/T of CsV₃Sb₅ as a function of H/H_{c2} , with bulk $H_{c2} = 0.16$ T. Similar data of the clean s -wave superconductor Nb (ref. ²²), the dirty s -wave superconducting alloy InBi (ref. ¹⁶), the multiband s -wave superconductor NbSe₂ (ref. ¹⁷), and an overdoped d -wave cuprate superconductor Tl-2201 (ref. ¹⁸) are shown for comparison.

Fig. 4 | Resistance under pressure and temperature - pressure phase diagram for CsV₃Sb₅. **a** Temperature dependence of resistance for CsV₃Sb₅ under various pressures up to 11.4 GPa. The curve of 0 GPa is from the CsV₃Sb₅ single crystal in Fig. 2b. **b** Temperature dependence of resistance for CsV₃Sb₅ under different magnetic fields at 0.8 GPa. Increasing the magnetic field gradually suppresses the superconducting transition. **c** Temperature - pressure phase diagram up to 11.4 GPa for CsV₃Sb₅. T_c is determined at the 10% drop of the normal-state resistance. It shows a clear superconducting dome.

d Temperature dependence of resistance for CsV₃Sb₅ under higher pressures up to 47.0 GPa. **e** Temperature dependence of resistance for CsV₃Sb₅ under different magnetic fields at 29.3 GPa. **f** Temperature - pressure phase diagram up to 47.0 GPa for CsV₃Sb₅. It shows two superconducting domes.